Journal of Molecular Structure 1230 (2021) 129920

Contents lists available at ScienceDirect

Journal of Molecular Structure

journal homepage: www.elsevier.com/locate/molstr

Design and synthesis of new benzopyrimidinone derivatives: α-amylase inhibitory activity, molecular docking and DFT studies

Sarra Chortani[a], Mabrouk Horchani[a], Mansour Znati[a], Noureddine Issaoui[b], Hichem Ben Jannet[a,*], Anis Romdhane[a,*]

[a] University of Monastir, Faculty of Science of Monastir, Laboratory of Heterocyclic Chemistry, Natural Products and Reactivity, Team: Medicinal Chemistry and Natural Products (LR11ES39), ChemistryDepartment, Avenue of Environment, 5019 Monastir, Tunisia
[b] University of Monastir, Faculty of Science of Monastir, Laboratory of Quantum and Statistical Physics (LR18ES18), PhysicsDepartment, Avenue of Environment, 5019 Monastir, Tunisia

ARTICLE INFO

Article history:
Received 5 September 2020
Revised 5 January 2021
Accepted 6 January 2021
Available online 11 January 2021

Keywords:
Benzopyrimidinones
Acyl chlorides
α-amylase activity
DFT
Docking

ABSTRACT

New benzopyrimidinone derivatives have been synthesized by reaction of 2-aminobenzamide with different acyl chlorides in good yield and their structures were confirmed by ^{1}H NMR, ^{13}C NMR and mass spectrometry. The newly synthesized compounds were studied theoretically by Density Functional Theory (DFT) method with 6–311++*G*(d, p) basis set, structural and some spectroscopic parameters were determined. The synthesized compounds were assessed for their in vitro α-amylase inhibitory activity. The structure-activity relationship (SAR) was discussed with the help of molecular docking analysis.

1. Introduction

Heterocyclic compounds containing nitrogen have attracted the interest of scientists in organic chemistry due to their abundance in natural products, their many fold applications and valuable as synthetic organic blocks [1-3]. The pyrimidinone ring is a useful structure in heterocyclic synthesis and it has demonstrated a significant range of biological properties such as antityrosinase [4], cytotoxic [5], antimicrobial [6], anti-proliferative [7], anti-acetylcholinesterase [8] andantidiabetic activities [9a-c] (Fig. 1). Moreover, many synthetic analogues of pyrimidine are also known to exhibit α-amylase inhibitory activity [10a-c] (Fig. 2).

Among the various classes of heterocyclic compounds, the benzopyrimidinone scaffold represents an important class of the nitrogen heterocycles and is established as a member of the privileged structural class particularly in medicinal chemistry [11]. They are found in structural core of more than 200 natural alkaloids isolated from plants, animals, and microorganisms [12]. The antimalarial Febrifugine, the cytotoxic Luotonin A, the sedative-hypnotic Methaqualone and the diuretic Metolazone [13] are representative examples of this family of natural and synthetic products (Fig. 3).

In view of the above mentioned findings and as continuation of our previous work, we have reported herein the synthesis of new derivatives of benzopyrmidinones for which the structural parameters were obtained by theoretical calculations using the Density Functional Theory (DFT) method with the common B3LYP function using 6–311++*G*(d, p) basis sets. Furthermore, molecular modeling studies of the all compounds **2a, 2b, 2c** and **2d** were also performed.

2. Materials and methods

2.1. Materials

All reactions were monitored by TLC using aluminum sheets of Merck silica gel 60 F_{254}, 0.2 mm. Melting temperatures were determined on an electrothermal 9002 apparatus and were reported uncorrected. NMR spectra were recorded on a Bruker AC-300 spectrometer at 300 MHz (^{1}H) and 75 MHz (^{13}C). All chemical shifts were reported as δ values (ppm) relative to residual non deuterated solvent. ESI-HRMS were acquired with an LCT Premier XE (Waters, ESI technique, positive mode) mass spectrometer.

* Corresponding authors.
E-mail addresses: hichem.bjannet@gmail.com (H.B. Jannet), anis_romdhane@yahoo.fr (A. Romdhane).

https://doi.org/10.1016/j.molstruc.2021.129920
0022-2860/

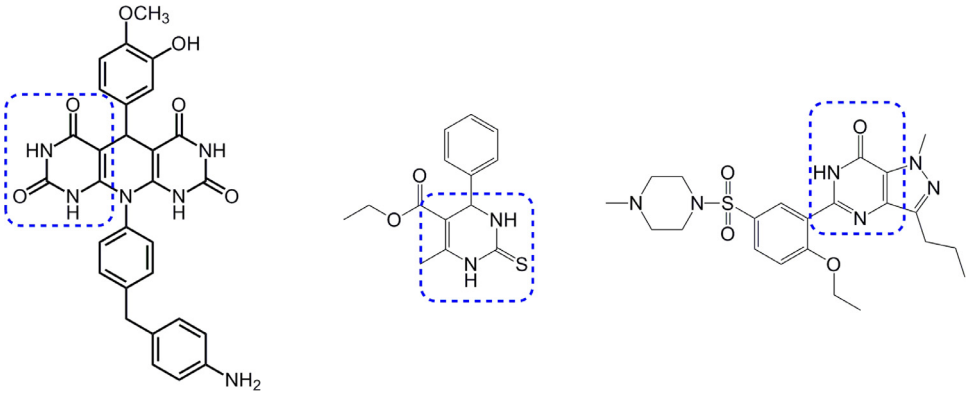

Fig. 1. Previously reported pyrimidinone derivatives as antidiabetic agents.

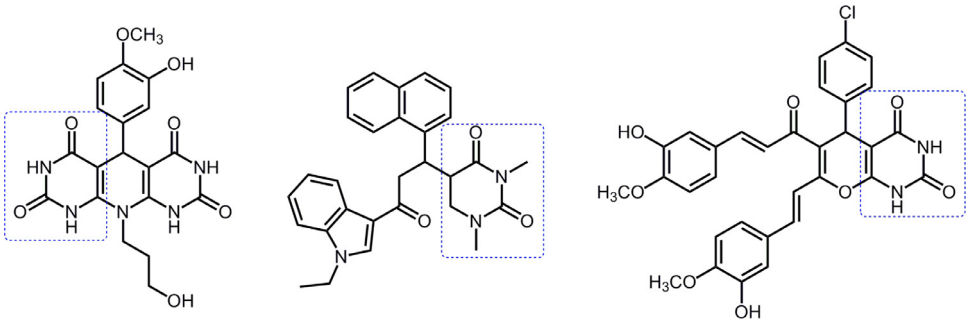

Fig. 2. Previously reported synthetic analogues of pyrimidine as α-amylase inhibitors.

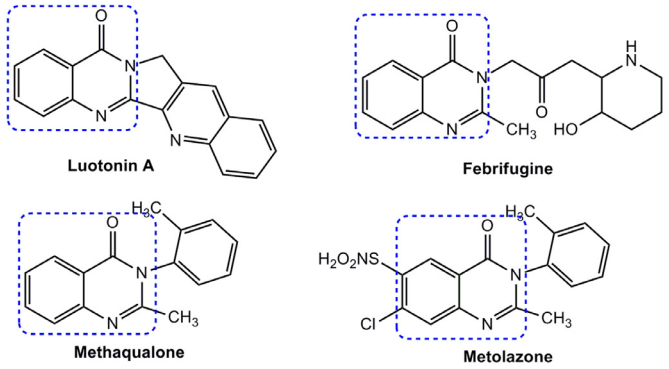

Fig. 3. Representative examples of natural and synthetic bioactive products with benzopyrimidinone cores.

2.2. Methods

2.2.1. General procedure for the synthesis of 2-benzopyrimidinones**2**

A mixture of 2-aminobenzamide **1** (1 g, 4.9 mmol) and acyl chloride (1 mL, 5.8 mmol) was heated at 80 °C for 1 hour on steam bath.After the reaction was completed, the mixture was cooled to room temperature and neutralized with Na_2CO_3 (10%) solution. The precipitate was collected and recrystallized from ethanol.

2.2.1.1.2-(chloromethyl)benzopyrimidin-4(3H)-one ***2a***. White solid, yield:80%. mp >300 °C. ES-HRMS $[M + H]^+$ calcd. for $(C_9H_8ClN_2O)^+$:195.0319, found: 195.0325. ^{1}H NMR (300 MHz, DMSO–d_6): δ (ppm) = 4.35 (s, 2H, H_9), 7.50 (t, J = 7.5 Hz, 1H, H_6), 7.64 (d, J = 8.1 Hz, 1H, H_8), 7.79 (t, J = 7.2 Hz, 1H, H_7), 8.09 (d, J = 7.8 Hz, 1H, H_5), 12.53 (s, 1H, NH). ^{13}C NMR (75 MHz, DMSO–d_6): δ (ppm) = 43.18 (C_9), 121.2 (C_{5a}), 125.8 (C_5), 127.0 (C_8), 127.0 (C_6), 134.5 (C_7), 148.1 (C_{8a}), 152.3 (C_2), 161.4 (C_4).

2.2.1.1.2. 2-(1-chloroethyl)benzopyrimidin-4(3H)-one ***2b***. White solid, yield:74%. Mp>300 °C.ES-HRMS $[M + H]^+$ calcd. for $(C_{10}H_9ClN_2O)^+$: 209.0480, found: 209.0484. ^{1}H NMR (300 MHz, DMSO–d_6): δ (ppm) = 1.84 (d, J = 6.6 Hz, 3H, H_{10}), 5.03 (q, J = 6.6 Hz, 1H, H_9), 7.53 (t, J = 7.3 Hz, 1H, H_6), 7.68 (d, J = 8.0 Hz, 1H, H_8), 7.81 (t, J = 7.4 Hz, 1H, H_7), 8.12 (d, J = 7.7 Hz, 1H, H_5), 12.54 (s, 1H, NH). ^{13}C NMR (75 MHz, DMSO–d_6): δ (ppm) = 21.72 (C_{10}), 55.4 (C_9), 121.9 (C_{5a}), 126.3 (C_5), 127.7 (C_8), 127.9 (C_6), 135.1 (C_7), 148.4 (C_{8a}), 155.4 (C_2), 162.0 (C_4).

2.2.1.3. 2-(dichloromethyl)benzopyrimidin-4(3H)-one ***2c***. White solid, yield:66%. mp: 218–220 °C. ES-HRMS $[M + H]^+$ calcd. for $(C_9H_7Cl_2N_2O)^+$: 228.9931, found: 228.9937. ^{1}H NMR (300 MHz, DMSO–d_6): δ (ppm) = 7.07 (s, 1H, H_9), 7.55(t, J = 7.4 Hz, 1H, H_6), 7.68 (d, J = 8.0 Hz, 1H, H_8), 7.81 (t, J = 7.5 Hz, 1H, H_7), 8.12 (d, J = 7.7 Hz, 1H, H_5), 12.54 (s, 1H, NH). ^{13}C NMR (75 MHz, DMSO–d_6): δ (ppm) = 67.9 (C_9), 122.0 (C_{5a}), 126.5 (C_5), 128.1 (C_8), 128.5 (C_6), 135.3 (C_7), 147.5 (C_{8a}), 151.8 (C_2), 161.8 (C_4).

2.2.1.4. 2-(chloro(phenyl)methyl) benzopyrimidin-4(3H)-one ***2d***. White solid, yield:72%. mp: 212–214 °C. ES-HRMS $[M + H]^+$ calcd. for $(C_{15}H_{13}ClN_2O)^+$: 271.0639, found: 271.0644. ^{1}H NMR (300 MHz, DMSO–d_6): δ (ppm) = 6.14 (s, 1H, H_9), 7.36–7.45 (m, 3H, H_{arom}), 7.52 (t, J = 7.5 Hz, 1H, H_6), 7.64–7.71 (m, 3H, H_{arom}), 7.81 (t, J = 7.6 Hz, 1H, H_7), 8.10 (d, J = 7.9 Hz, 1H, H_5), 12.67 (s, 1H, NH). ^{13}C NMR (75 MHz, DMSO–d_6): δ (ppm) = 59.7 (C_9), 121.5 (C_{5a}), 126.3 (C_5), 127.8 (C_8), 127.9 (C_6), 128.6 ($C_{12,14}$), 129.0 ($C_{11,15}$),129.4 (C_{13}), 135.2 (C_7), 137.2 (C_{10}),148.4 (C_{8a}), 154.3 (C_2), 161.9 (C_4).

2.2.2. In vitro α-amylase inhibition assay

The α-amylase inhibitory assay of the tested compounds was evaluated according to a previously described method (Ranilla et al., 2010) [14] with some modifications. In brief, 0.5 mL of each

compound (in DMSO) was mixed with 0.5 mL of α-amylase solution (0.5 mg/mL) with 0.02 M sodium phosphate buffer (pH 6.9 with 0.006 M NaCl). The mixture was incubated at room temperature for 10 min and 0.5 ml of starch solution (1%) in 0.02 M sodium phosphate buffer (pH 6.9 with 0.006 M NaCl) was added. The resulting mixture was incubated at room temperature for 10 min, and the reaction was terminated using 1 mL of dinitrosalicylic acid color reagent. At this time, the test tubes were placed in a water bath (100 °C and 5 min) and cooled until room temperature was reached. The mixture was then diluted with 10 mL of deionized water, and absorbance was determined at 540 nm. The absorbances of blank (buffer and DMSO instead of the tested compound and amylase solution) and control (buffer and DMSO instead of the tested compound) samples were also determined. Acarbose was used as a positive control. The inhibition of α-amylase was calculated using the following equation:

$$\% \text{ inhibition of } \alpha\text{-Amylase} = (Abs_{control} - Abs_{sample}) /(Abs_{control}) \times 100$$

Where $Abs_{control}$ corresponds to the absorbance of the solution containing only α-amylase and the buffer instead of the compound, and Abs_{sample} corresponds to the absorbance of the solution in the presence of both tested compound and α-amylase. Compound concentration providing 50% inhibition (IC_{50}) was obtained plotting the inhibition percentage against the concentrations of the tested compound. The tests were carried out in triplicate.

2.2.3. Molecular docking procedure

Molecular docking simulations were performed by the Auto Dock 4.2 program package [15]. The optimization of all the geometries of scaffolds was performed with ACD (3D viewer) software (http://www.filefacts.com/acd3d-viewer-freeware-info). The crystal structures of PDB (PDB: 4W93) was obtained from the RSCB protein data bank [16]. First, the water molecules were eliminated and the missing hydrogens and Gasteiger charges were then added to the system during the preparation of the receptor input file. Indeed, Auto Dock Tools were used for the preparation of the corresponding ligand and protein files (PDBQT). Next, pre-calculation of the grid maps was carry out using Auto Grid for saving a lot of time during docking. Subsequently, the docking calculation was performed using a grid per map with 40 × 40 × 40 Å points in addition to grid-point spacing of 0.375 Å, which was centered on the receptor in order to define the active site. After complex formation, the visualization and analysis of interactions were performed using Discovery Studio 2017R2 (https://www.3dsbiovia.com/products/collaborative-science/biovia-discovery-studio/).

2.2.4. Computational details (DFT studies)

Density functional theory plays an important role in determining the molecular electronic structure by computer simulations. The studied products were modelled with the *Gauss View* program [17] and, later optimized with the Gaussian 09 program [18] by using the functional hybrid (Becke, three-parameter, Lee-Yang-Parr) B3LYP with the 6–311++*G*(d, p) basis set [19, 20]. Thermodynamic parameters and molecular electrostatic potentials were predicted at the same level of theory. Additionally, reactivities and behaviors of the studied products were predicted by using calculations of frontier orbitals and the chemical potential (μ) electronegativity (χ), global softness (S), global hardness (η), global electrophilicity index (ω) and nucleophilicity indexes (E) descriptors [21-23].

2.2.5. Statistical analysis

Data from the bioassay carried out were subjected to analysis of variance (ANOVA) using SPSS 16.0 for Windows. The inhibition data of α-amylase activity of compounds **2a-d** have been transformed using arcsin- square root (arcsin$\sqrt{x}$) transformation before ANOVA. Means were separated at the 5% significance level by a least significant difference test (*Student's* test).

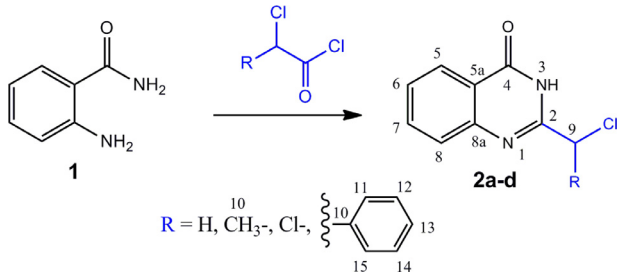

Scheme 1. Synthetic pathway to benzopyrimidinone derivatives.

3. Results and discussion

3.1. Synthesis

The synthetic strategy adopted to obtain the target compounds are depicted in Scheme 1.The synthesis of new benzopyrimidinone derivatives was done by the chloroacylation of 2-aminobenzamide **1** using various acyl chloride on steam bath for one hour followed by treatment with sodium carbonate solution [24]. The formed compounds were characterized according to their spectral data.

In fact, the ^{1}H NMR spectrum of compound **2b**, as an example, showsa doublet at δ_H 1.84 (J = 6.6 Hz) relative to the methyl group and a quadruplet at δ_H 5.03 (J = 6.6 Hz) attributable to the methane proton, both introduced by the 2-chloropropanoyl chloride, and the presence a characteristic singlet at δ_H 12.54 assignable to the mobile proton –NH. The remarkable de-shielding of the methine proton isexplained by the inductive attractor effect exerted by the neighboring chlorine atom and the two nitrogen atoms of the pyrimidinone ring (one hybridized sp^2 attarctor, and the other conjugated with the carbonyl function), thus leaving a partial positive charge on the sp^2 quaternary carbone directly linked to the methine. Moreover, the exploration of the ^{13}C NMR spectrum allowed to notes the appearance of new signals at δ_C 21.7 and 55.4 due to carbons C_9 and C_{10}, respectively.

Finally, the ES-HRMS of this compounds howed a pseudo-molecular ion peak $[M + H]^+$at *m/z* 209.0484 in agreement with its molecular formula $(C_{10}H_9ClN_2O)^+$.

3.2. In vitro α-amylase inhibitory activity

The in vitro α-amylase inhibitory activity of compounds **2a-d** were assessed by measuring the inhibition percentage (PI%). As shown in Table 1, the evaluated compounds exhibited significant inhibitory potentials towards α-amylase with IC_{50} values ranging from 60 to 31 μg/mL compared to acarbose used as a positive control (IC_{50}=29.86 ± 1.57 μg/mL). Compound **2a**(-CH_2–Cl), was found to be the less active derivative with an IC_{50}value of 60.07 ± 1.89 μg/mL. On the other hand, it has been found that the compound **2b** (CH_3–CH–Cl) exhibited the highest α-amylase inhibition activity with an IC_{50} value of 31.12 ± 1.05 μg/mL, comparable to that of acarbose. The significant activity of compound **2b** compared to that of its analogue **2a** is certainly due to the additional methyl group which, by its inductive donor effect and its spatial arrangement in this position, could promote this activity. The compound **2c** (Cl-CH–Cl) was found to be more active than **2a**. This finding clearly shows the contribution of the two chlorine atoms to this activity. On the other hand, the comparison of the activity of derivative **2c** with that of **2b** shows that the substitution of the methyl group in the latter by a second chlorine atom (compound **2c**) did not improve this activity

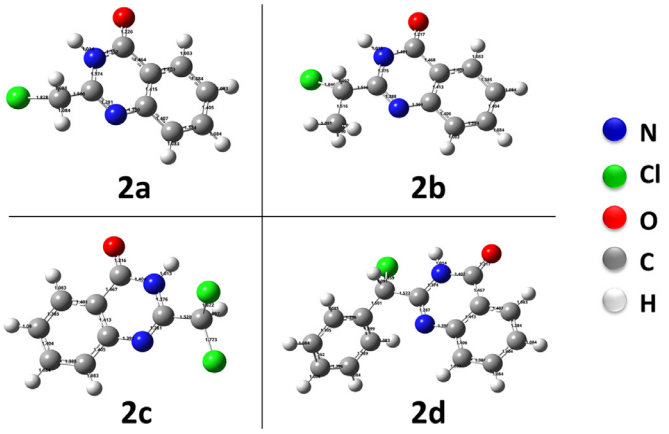

Fig. 4. Optimized geometries of the products 2a-d at B3LYP/6–311++*G*(d, p) level of DFT.

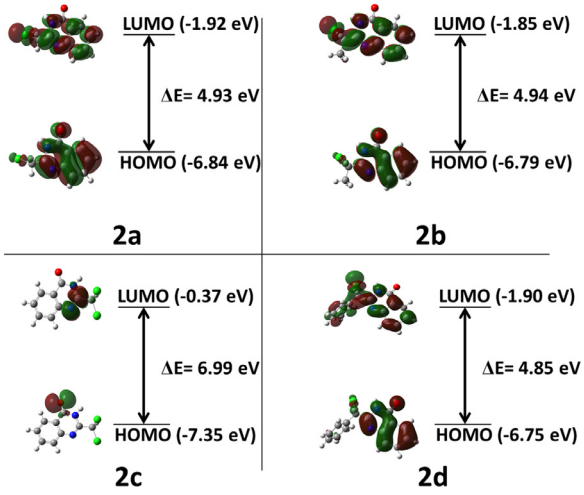

Fig. 5. HOMO, LUMO orbitals and their energy gap (ΔEgap) of the products 2a-d at B3LYP/6–311++*G*(d, p) level of DFT.

(IC_{50} = 37.22 ± 1.32μg/mL). The size of the added chlorine atom in **2c** and GLU-A-233. For more details, its inductive attracting effect unlike that of the methyl group in **2b** could be at the origin of this difference in activity.

The introduction of a phenyl group in compound **2d** decreased the activity (IC_{50} = 43.14 ± 2.05μg/mL) by comparison to **2c**. This result shows that the relatively higher inductive attracting effect exerted by the second chlorine atom in **2c** compared to that exerted by the phenyl group in **2d**, may explain the attenuation of this activity. Also, it is possible to think at the steric hindrance of the phenyl group in compound **2d** which could possibly explain the loss of this activity compared to that of **2b** with a methyl group. The compound **2d** remains still more active than its analogue **2a**.

3.3. DFT studies

3.3.1. Geometry optimization and reactivity parameters

Optimized structures obtained by DFT method using B3LYP hybrid functional with 6–311++*G* (d, p) basis set of 2-(chloroalkyl)quinazolin-4(3*H*)-one derivatives **2a-d** are shownin Fig. 4. Several thermodynamic parameters such as the energy (*E*), enthalpy (Δ, *H*°), entropy (*S*) , heat capacity (C_y) , dipole moment and thermal energy were calculated using B3LYP functional with 6–311++*G*(d, p) basis set. The calculated parameters of compounds **2a-d** are given in Table 2. Compound **2d** with a phenyl ring was found to have the highest dipole moment (3.734 Debye) while compound **2c** with an extra chlorine atom gave the lowest dipole moment (1.70 Debye). In order to compute the electronic properties of the studied compound, a powerful practical approach has been carried out for describing the chemical reactivity, namely the Frontier Molecular Orbital (FMO) theory. The FMO's also plays a very crucial role in various fields such as optical, electric properties and field of quantum chemistry. Various reactivity descriptors like electron affinity $^{(A)}$, ionization potential *(I)*, hardness (η), electronegativity (χ), dimensionless descriptor(ε) as well as electrophilicity index (ω), all derived from the HOMO and LUMO energies, were proposed for understanding many aspects of reactivity associated to chemical reactions and describe the chemical hardness and stability of compounds [25] all these parameters are calculated and given in Table 3. Recall that, the highest occupied molecular orbital (HOMO) and lowest unoccupied molecular orbital (LUMO) are fundamental quantum chemical descriptors and can be used to predict stability and reactivity of molecules [26, 27]. The band gap HOMO-LUMO specifies the lowest energy needed for an electron to transits from the valence band to the conduction band also determines the biological activity from intramolecular charge transfer. However, in a typical system, the HOMO act as an electron donor and the LUMO primarily act as the electron acceptor [26, 27].

For more detail, in these parameters, *(I)* and *(A)* are the ionization potential and electron affinity of the molecule, respectively. Indeed, the ionization potential *(I)* characterizes the susceptibility of a molecule, whereas the electron affinity of the molecule *(A)* refers to the capability of a ligand to accept one electron from a donor. As can be seen from Table 3, the ionization potential *(I)* value of compound **2c** (7.35 eV) indicates the greater donating capability of **2c** (*R*= Cl) as compared to its analogs. The lower value of *(A)* (0.37 eV) of derivative **2c**, shows its greater acceptability, unlike compound **2a** (*R* = *H*) which has the highest electron affinity value (1.92 eV). From a general point of view, the all positive values noted for these compounds (**2a-d**) are a good indication of their possible use in charge transfer reactions. In addition, when the value of the global hardness (η) is showed greater, this explains that the compound in question is more stable and less reactive. So, it is the case of the derivative **2c** with (η) value of 3.49 eV while the compound **2d** (*R*= pH) exhibiting the lower value (2.43 eV) is therefore considered to be the less stable and more reactive. Another quantum descriptors which is extensively used: electronegativity (χ) and the electrophilicity (ω). This last factor has been proposed as a means of measuring the decrease in energy due to the maximum flow of electrons between the donor and the acceptor. Compound **2c** displaying the lowest values demonstrates the above findings concerning stability and reactivity.

3.3.2. Frontier molecular orbital (FMO) analysis

The frontier molecular orbitals, HOMO (highest occupied molecular orbital) and LUMO (lowest unoccupied molecular orbital), play a significant role in defining the reactivity of molecules as well as charge delocalization within the molecule. The orbital HOMO is capable to give electrons, while (LUMO) can take electrons first [28]. Meanwhile, Figs. 5 and 4 show the Frontier Molecular Orbital (FMO) of compounds **2a-d**. This analysis shows that the HOMO orbital is mainly concentrated on all structure of compound **2a**, on almost the entire structure except the methyl group of compound **2b**, on the oxygen (carbonyl groups) of compound **2c** and is localized on 2-(chloromethyl)quinazolin-4(3*H*)-one fragment and the chlorine atom of derivative **2d** However, strong delocalization of the LUMO for compound **2a** occurs on the whole structure except the carbonyl groups. Similarly, for compound **2b** inaddition to methyl groups, the LUMO is concentrated especially on the nitro-

gen atoms of derivative **2c** and is centered on total structure unless carbonyl groups of compound **2d**

On the other hand, the energy gap which expresses the energy difference between this two important FMOs (HOMO-LUMO), signifies the chemical hardness-softness, the kinetic stability and the reactivity of a molecule [29, 30]. Hard molecules with large HOMO-LUMO gap are more stable and less reactive. In the opposite case, soft molecules having a small HOMO-LUMO gap are more reactive and less stable [31]. In this light and for given in Fig. 8, compound **2c** having the highest energy gap (6.99 eV) is the most hard and stable and less reactive, thus the insertion of chlorine exerting an electron withdrawing effect increases the stability of the molecule unlike compounds **2a, 2b** and **2d**

3.3. 3. molecular electrostatic potential (MEP)

The molecular electrostatic potential (MEP) surface describes the intensity of potential at different regions in the molecular structure, hence the behavior and the reactivity of the molecules. More precisely, it is widely used to predict the nucleophilic and electrophilic active sites of compounds. The positive (assigned to blue) districts of MEP were related to nucleophilic attack while the negative (assigned to red and yellow) regions explain the electrophilic reactivity [32, 33]. All these interesting properties motivated us to do the MEP mapping of synthesized compounds **2**. It can be seen from Fig. 6, the NH group shows positive potential and hence suitable site for nucleophilic attack. While the negative potential shows that the high electron density is located on the carbonyl function juxtaposed to the NH group, the latter can therefore attack in two ways: either on the electrophilic site of another molecule (intermolecular attack) or on the electrophilic site of the carbonyl function of the same molecule (intramolecular attack), as it has been already described. In the latter case, the oxygen atom will be too electronegative, which makes it susceptible to attack another molecule. All the above results showed the good reactivity of the synthesized compounds **2**. The last findingis also verified bythe frontier molecular orbitals analysis HOMO, LUMO and the energy gap.

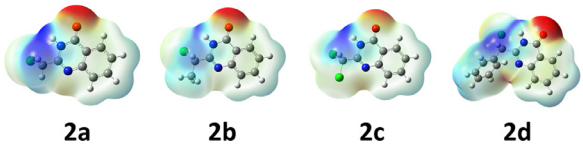

Fig. 6. Molecular electrostatic potential (MEP) surfaces of the products 2a-d at B3LYP/6–311++*G*(d, p) level of DFT.

3.4. Molecular docking study

To better explain the obtained α-amylase inhibition activity (Table 1) and the mechanism of action of the compounds, the binding modes of all representative ligands, **2a, 2b, 2c** and **2d** in addition to the control (acarbose) using the docking program, AutoDock 4.2 package with Discovery Studio 2017R2, have

Table 1
α-Amylase inhibitory activity of compounds **2a-d**.

Compound	Structure	IC_{50} ($\mu g/mL$)[a]
2a	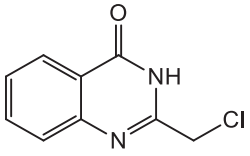	60.07 ± 1.89
2b	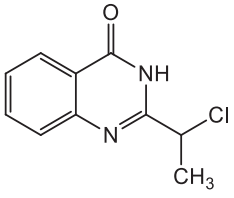	31.12 ± 1.05
2c	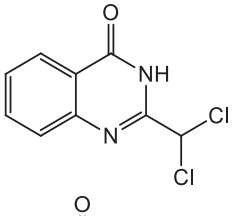	37.22± 1.32
2d	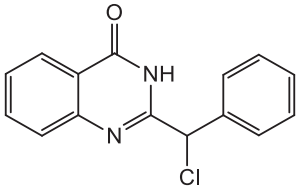	43.14 ± 2.05
Acarbose[b]		29.86± 1.57

a The concentration at which 50% of α-amylase is inhibited (mean ± SD, $n = 3$).
b Positive control.

Table 2
The calculated thermodynamic parameters (at 298.15 K) for the synthesized products **2a-d** with DFT/B3LYP method using 6–311++*G*(d, p) basis set.

Compounds	E (kJ.mol^{-1})	$^{\Delta, H}$ (298) (Kcal/mol)	Thermal energy (kcal mol^{-1})	C_v (cal mol^{-1}K^{-1})	S (cal mol^{-1} K^{-1})	Dipole moment (Debye)
2a	−2,605,326.59	338,453.79	98.954	39.466	102.19	3.397
2b	−2,708,550.02	338,461.19	117.352	45.137	108.545	3.238
2c	−3,811,996.03	338,461.25	93.59	43.087	110.298	1.70
2d	−3,212,057.42	338,462.76	152.22	58.65	127.653	3.734

Table 3
Calculated kinetic parameters of the reaction forthe synthesized products **2a-d** at B3LYP/6–311++*G*(d, p) level of DFT.

Compounds	E_{HOMO} (eV)	E_{LUM} (eV)	$\Delta E_{(HOMO-LUMO)}$ (eV)	*I* (eV)	*A* (eV)	η (eV)	χ (eV)	ω (eV)	ε
2a	−6.84	−1.92	4.93	6.84	1.92	2.46	4.38	3.90	−0.89
2b	−6.79	−1.85	4.94	6.79	1.85	2.47	4.32	3.78	−0.88
2c	−7.35	−0.37	6.99	7.35	0.37	3.49	3.86	2.13	−0.55
2d	−6.75	−1.90	4.85	6.75	1.90	2.43	4.32	3.85	−0.89

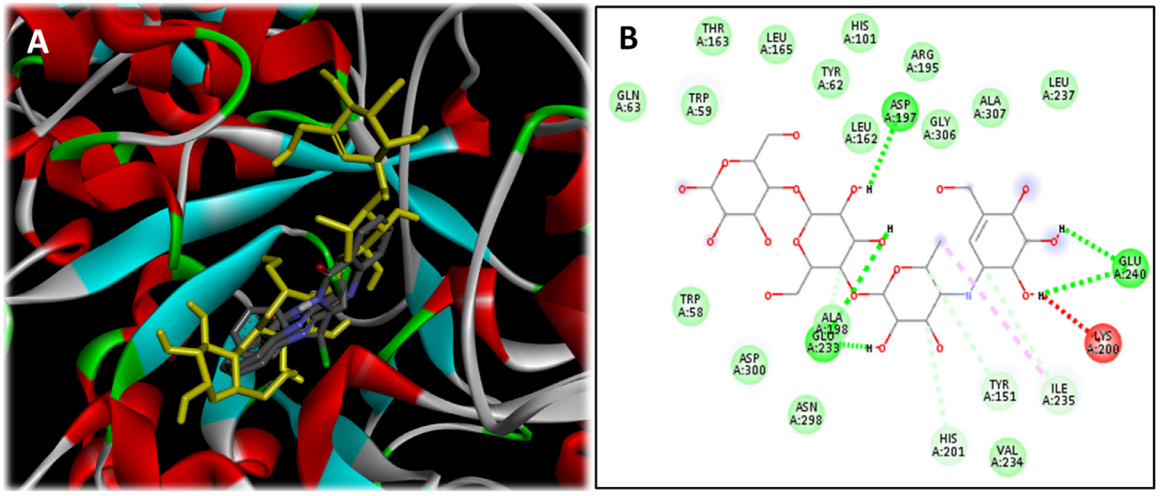

Fig. 7. A: Superimposed conformations of best docked poses for respective ligands 2 (grey color) and acarbose (yellow color) in the cleft of α-amylase pocket, B: 2D-interactions of the standard drug acarbose in the active site of PDB: 4W93. (For interpretation of the references to colour in this figure legend, the reader is referred to the web version of this article.)

Table 4
Binding energies of promising anti-α-amylase agents.

Compound	Binding energy (kcal/mol)
2a	−5.4
2b	−6.2
2c	−6.0
2d	−6.1
acarbose	−6.2

been examined. The α-amylase-acarbose inhibitor complex showed −6.2 kcal/mol binding energy containing mostly four hydrogen bonds with the interacting residues ASP-A-179, GLU-A-233, GLU-A-240 (Figs.7-A and B).

On another hand, the most anti-α-amylase derivative **2b**, presenting the lower free binding energy, compared to those of its analogues and equal to that of the control (Table 4), interacted with the active site of the enzyme *via* the most marked interactions: tow hydrogen bonding (green color) by its NH and carbonyl groups with GLU-A-233 and ARG-A-195 besides to Pi-Anion interaction (golden color) with ASP-A-197 (Fig. 8). These findings reinforce the considerable activity of this derviative (**2b**) (IC_{50}: 31.12 ± 1.05 μg/mL)compared to its analogues. The low free binding energy value and the hydrogen bonds engaged with the enzyme are proof of the inhibitory potential of compound **2b** compared to the other compounds.

In the case of **2a, 2c, 2d**-α-amylase complexes (Fig. 8), we found that these compounds formed a hydrogen bond with GLU-A-233. For more details, the derivative **2a** displayed a Pi-Anion interaction with ASP-A-300 and a Pi-Pi shaped (dark pink color) with TYR-A-62. The compound **2c** showed a carbon hydrogen bond (grey color) with ALA-A-198, a Pi-Anion with GLU-A-233, a Pi-Alkyl (light pink color) with LEU-A-162, ALA-A-198 and LYS-A-200, a Pi-Pi stacked (dark pink color) with TYR-A-151, a Pi-Pi shaped with HIS-A-201, and Pi-Sigma interactions (dark purple color) with ILE-A-235. On the other hand, compound **2d** established interactions with residues LEU-A-162 and ALA-A-198 (*via* Pi-Alkyl), TYR-A-62 (*via* Pi-Pi stacked), HIS-A-201 (*via* Pi-Pi shaped), ASP-A-197 (*via* Pi-Anion) and HIS-A-101 (*via* carbon hydrogen bond).

The docking calculation were found in good agreement with the experimental results which show the most marked anti-α-amylase activity of compound **2b** compared to its analogues.

4. Conclusion

In conclusion, this work describes the synthesis andthe structural elucidation of a series of new benzopyrimidinones derivatives **2a-d**, *via* cyclocondensation reaction of 2-aminobenzamide with different acyl chlorides. The newly prepared compounds **2a-d** have been screened for their α-amylase inhibitory activity. Further-

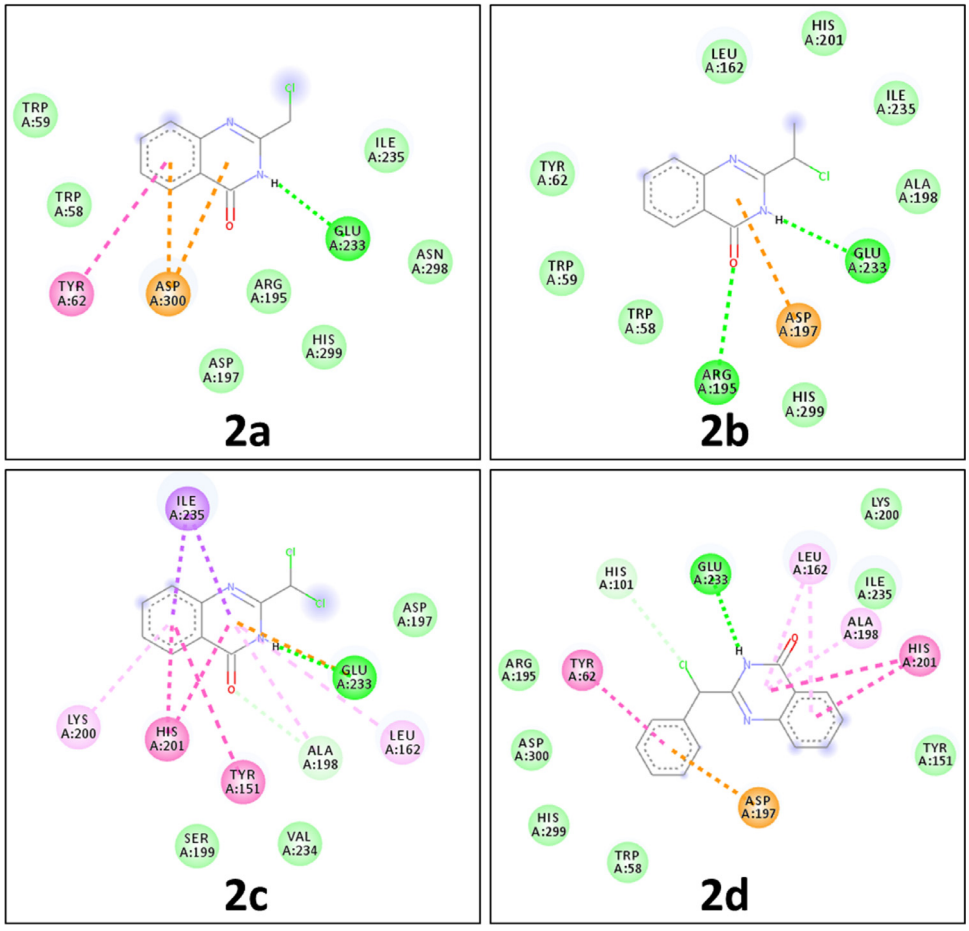

Fig. 8. Binding pose of conjugates 2a, 2b, 2c and 2d in the active site of PDB: 4W93.

more, all synthesized compounds were modeled by DFT calculations using 6–311++G(d, p) basis set, the geometrical parameters and frontier molecular orbital have been obtained and analyzed, the energy gap between the HOMO and LUMO molecular orbitals allowed to determine the chemical stability and electrical transport properties of derivatives **2a-d**. The molecular electrostatic potential has been mapped for predicting sites and relative reactivities towards electrophilic and nucleophilic attacks which opens up the possibilities to think about other chemical reactions starting from precursors**2**. Molecular docking simulations exhibited excellent bindings of the synthesized compounds with the receptor active sites of PDB: 4W93. The multiple interactions made by compound **2b** with this enzyme used, clearly confirmed its significant activity compared to its analogues.

The above significant findings showed that compounds **2a-d** may be of interest for further studies of the mechanism of action, binding and biological profile of the promising tested compounds.

Credit author statement

Sarra Chortani did the synthesis work. Mabrouk Horchani did the Docking party. Mansour Znati tested the α-amylase activity. Noureddine Issaoui performed the DFT study. Hichem Ben Jannet contributed to the discussion of the results and completed the redaction of the manuscript. Anis Romdhane was the supervisor of the present work, he also checked the structure determination of the synthesized compounds and the biological study, and he completed the redaction of the article.

Declaration of Competing Interest

None declared.

Acknowledgments

The authors are grateful to the Ministry of Higher Education and Scientific Research of Tunisia for financial support to the Laboratory of Heterocyclic Chemistry, Natural Products and Reactivity (LR11ES39).

Supplementary materials

Supplementary material associated with this article can be found, in the online version, at doi:10.1016/j.molstruc.2021.129920.

References

[1] M. Jha, S. Guy, Y.C. Ting, Microwave assisted synthesis of indole-annulated dihydropyrano[3,4-*c*]chromene derivatives via hetero-Diels–Alder reaction, Tetrahedron Lett 52 (2011) 4337–4341.
[2] H.A. Hasan, E. Abdulmalek, T.A. Saleh, M.B. Abdul Rahman, K.B. Shaari, B.M. Yamin, K.W. Chan, Synthesis of novel 6-substituted-5,6-Dihydrobenzo[4,5] Imidazo[1,2-c] quinazoline compounds and evaluation of their properties, J. Mol. Struct. 1193 (2019) 482–494.
[3] S. Singh, L.K. Sharma, A. Saraswat, I.R. Siddiqui, H.K. Kehrib, R.K. Pal Singh, Electrosynthesis and screening of novel 1,3,4-oxadiazoles as potent and selective antifungal agents, R. S. C. Adv. 3 (2013) 4237–4245.
[4] R. Wang, W.M. Chai, Q. Yang, M.K. Wei, Y. Peng, 2-(4-Fluorophenyl)-quinazolin-4(3H)-one as a novel tyrosinase inhibitor: synthesis, inhibitory activity, and mechanism, Bioorg. Med. Chem. 24 (2016) 4620–4625.

[5] D. Kumar, G. Mariappan, A. Husain, J. Monga, S. Kumar, Design, synthesis and cytotoxic evaluation of novel imidazolone fused quinazolinone derivatives, Arab. J. Chem. 10 (1) (2017) 344–350.

[6] K.P. Rakesh, H.K. Kumara, B.J. Ullas, J. Shivakumara, D.C. Gowda, Amino acids conjugated quinazolinone-Schiff's bases as potential antimicrobial agents: synthesis, SAR and molecular docking studies, Bioorg. Chem. 90 (2019) 10309.

[7] R. Bollu, S. Banu, S. Kasaboina, R. Bantu, L. Nagarapu, S. Polepalli, N. Jain, Potential anti-proliferative agents from 1,4-benzoxazinone-quinazolin-4(3H)-one templates, Bioorg. Med. Chem. Lett. 27 (2017) 5481–5484.

[8] Y. Zhu, L.Y. Zhou, Y.R. Jiang, X.J. Zhao, D. Guo, Design, synthesis and biological evaluation of dual acetylcholinesterase and phosphodiesterase 5A inhibitors in treatment for Alzheimer's disease, Bioorg. Med. Chem. Lett. 27 (2017) 4180–4184.

[9] a)F. Panahi, R. Yousefi, M. H. Mehraban, A. Khalafi-Nezhad, Synthesis of new pyrimidine-fused derivatives as potent and selective antidiabetic α-glucosidase inhibitors, Carbohydr. Res. 380 (2013) 81-91.; b)K. L. Dhumaskar, S. Nandan Meena, S. C. Ghadi, S. G. Tilve, Graphite catalyzed solvent free synthesis of dihydropyrimidin-2(1H)-ones/thiones and their antidiabetic activity, Bioorg. Med. Chem.Lett. 24 (2014) 2897-2899.; c)B. N. Reddy, R. Raju. Ruddarraju, G. Kiran, M. Pathak, A. R. NarsimhaReddy, NovelPyrazolo[3,4-d]pyrimidine-Containing Amide Derivatives: Synthesis, Molecular Docking, In Vitro and In Vivo Antidiabetic Activity, Med. Chem. Drug Disco. 4 (2019) 10072-10078.

[10] a)S. Shahidpour, F. Panahi, R. Yousefi, M. Nourisefat, M. Nabipoor, A. Khalafi-Nezhad, Design and synthesis of new antidiabetic α-glucosidase and α-amylase inhibitors based on pyrimidine-fused heterocycles, Med. Chem. Res. 24 (2015) 3086-3096.; b)Yousefi, R. Yousefi, F. Panahi, S. Sarikhani, A. Zolghadr, A. Bahaoddini, A. Khalafi-Nezhad, Novel curcumin-based pyrano[2,3-d]pyrimidine anti-oxidant inhibitors for α-amylase and α-glucosidase: Implications for their pleiotropic effects against diabetes complications, Int. J. Biol. Macromol. 78 (2015) 46-55.; c)F. A. Badria, S. Atef, A. M. Al-Majid, M. Ali, Y. A. M. M. Elshaier, H. A. Ghabbour, M. S. Islam, A. Barakat, Synthesis and Inhibitory Effect of Some Indole-Pyrimidine Based Hybrid Heterocycles on α-Glucosidase and α-Amylase as Potential Hypoglycemic Agents, ChemistryOpen. 8 (2019) 1288-1297.

[11] V. Gupta, S.K. Kashaw, V. Jatav, P. Mishra, Synthesis and antimicrobial activity of some new 3–[5-(4-*substituted*) *phenyl*-1,3,4-*oxadiazole*-2*yl*]-2- styrylquinazoline-4(3H)-ones, Med.Chem. Res. 17 (2008) 205–211.

[12] S.B. Mhaske, N.P. Argad, The chemistry of recently isolated naturally occurring quinazolinone alkaloids, Tetrahedron 62 (2006) 9787–9826.

[13] S.K.P ulakhandam, N.K. Katari, S.B. Jonnalagadda, Design and synthesis of novel 6-substituted quinazoline-2-thiols, Mol. Divers. 23 (2019) 351–360.

[14] L.G. Ranilla, Y.I. Kwon, E. Apostolidis, K. Shetty, Phenolic compounds, antioxidant activity and in vitro inhibitory potential against key enzymes relevant for hyperglycemia and hypertension of commonly used medicinal plants, herbs and spices in Latin America, Bioresour. Technol. 101 (2010) 4676–4689.

[15] O. Trott, A.J. Olson, AutoDock Vina: improving the speed and accuracy of docking with a new scoring function, efficient optimization, and multithreading, J. Comput. Chem. 31 (2010) 455–461.

[16] L.K. Williams, X. Zhang, S. Caner, C. Tysoe, N.T. Nguyen, J. Wicki, D.E. Williams, J. Coleman, J.H. McNeill, V. Yuen, R.J. Andersen, S.G. Withers, G.D. Brayer, The amylase inhibitor montbretin A reveals a new glycosidase inhibition motif, Nat. Chem. Biol. 11 (2015) 691–696.

[17] R. Dennington, T. Keith, J. Millam, KS Mission (Ed.), Version 5, Semichem Inc., Shawnee, 2009.

[18] M.J. Frisch, G.W. Trucks, H.B. Schlegel, G.E. Scuseria, M.A. Robb, J.R. Cheeseman, G. Scalmani, V. Barone, B. Mennucci, G.A. Petersson, H. Nakatsuji, M. Caricato, X. Li, H.P. Hratchian, A.F. Izmaylov, J. Bloino, G. Zheng, J.L. Sonnenberg, M. Hada, M. Ehara, K. Toyota, R. Fukuda, J. Hasegawa, M. Ishida, T. Nakajima, Y. Honda, O. Kitao, H. Nakai, T. Vreven Jr., JA. Montgomery, J.E. Peralta, F. Ogliaro, M. Bearpark, J.J. Heyd, E. Brothers, K.N. Kudin, V.N. Staroverov, T. Keith, R. Kobayashi, J. Normand, K. Raghavachari, A. Rendell, J.C. Burant, S.S. Iyengar, J. Tomasi, M. Cossi, N. Rega, J.M. Millam, M. Klene, J.E. Knox, J.B. Cross, V. Bakken, C. Adamo, J. Jaramillo, R. Gomperts, R.E. Stratmann, O. Yazyev, A.J. Austin, R. Cammi, C. Pomelli, J.W. Ochterski, R.L. Martin, K. Morokuma, V.G. Zakrzewski, G.A. Voth, P. Salvador, J.J. Dannenberg, S. Dapprich, A.D. Daniels, O. Farkas, J.B. Foresman, J.V. Ortiz, J. Cioslowski, D.J. Fox, GAUSSIAN 09, Revision E.01, Gaussian, Inc, Wallingford, 2013.

[19] A.D. Becke, Becke's three parameter hybrid method using the LYP correlation functional, J. Chem. Phys. 98 (1993) 5648–5652.

[20] C. Lee, W. Yang, R.G. Parr, Density-functional exchange-energy approximation with correct asymptotic behavior, Phys. Rev. B. 37 (1988) 785–789.

[21] R.G. Parr, R.G. Pearson, Electronegativity and bond energy, J. Am. Chem. Soc. 105 (1983) 7512–7516.

[22] N. Issaoui, H. Ghalla, F. Bardak, M. Karabacak, N. AouledDlala, H.T. Flakus, B. Oujia, Combined experimental and theoretical studies on the molecular structures, spectroscopy, and inhibitor activity of 3-(2-thienyl)acrylic acid through AIM, NBO,FT-IR, FT-Raman, UV and HOMO-LUMO analyses, and molecular docking, J. Mol. Struc. 1130 (2017) 659–668.

[23] N. Issaoui, H. Ghalla, S.A. Brandan, F. Bardak, H.T. Flakus, A. Atac, B. Oujia, Experimental FTIR and FT-Raman and theoretical studies on the molecular structures of monomer and dimer of 3-thiopheneacrylic acid, J. Mol. Struct. 1135 (2017) 209–221.

[24] A.M. Elkhawaga, A.M. Kamal El-Dean, Sh.M. Radwan, M.M. Ahmed, Synthesis of Some Imidazopyrazolopyrimidines, Pyrazolopyrimidopyrimidines and Pyrazolopyrimidothiazines, Bull. Korean Chem. Soc .30 (2009) 561–566.

[25] C.A.Mebi, DFT study on structure, electronic properties, and reactivity of cis-i-somers of [(NC5H4-S)2Fe(CO)2], J. Chem. Sci. 123 (2011) 727–731.

[26] O. Noureddine, S. Gatfaoui, S.A. Brandán, H. Marouani, N. Issaoui, Structural, docking and spectroscopic studies of a new piperazine derivative, 1-Phenylpiperazine-1,4-diium bis(hydrogen sulfate, J. Mol. Struct 1212 (2020) 127351.

[27] H. Ghalla, N. Issaoui, F. Bardak, A. Atac, Intermolecular interactions and molecular docking investigations on 4-methoxybenzaldehyde, Comput. Mat. Science 149 (2018) 291–300.

[28] X.H. Liu, L. Pan, C.X. Tan, J.Q. Weng, B.L. Wang, Z.M. Li, Synthesis, Biological Activities and DFT Calculation of a-Aminophosphonate Containing Cyclopropane Moiety, Asian. J. Chem. 23 (2011) 4031–4036.

[29] B. Kosar, C. Albayrak, Spectroscopic investigations and quantum chemical computational study of (E)-4-methoxy-2-[(*p-tolylimino*)*methyl*]phenol, Spectrochim. Acta. 78 (2011) 160–167.

[30] A.M. Asiri, M. Karabacak, M. Kurt, K.A. Alamry, Synthesis, molecular conformation, vibrational and electronic transition, isometric chemical shift, polarizability and hyperpolarizability analysis of 3-(4-Methoxy-phenyl)-2-(4-nitro-phenyl)-acrylonitrile: a combined experimental and theoretical analysis, Spectrochim Acta 82 (2011) 444–455.

[31] H. Tanak, Density functional computational studies on 2-[(2, 4-D*imethylphenyl*) *iminomethyl*]-3, 5-dimethoxyphenol, Int. J. Quant. Chem. 112 (2012) 2392–2402.

[32] L.W. Li, C.J. Wu, Z.Q. Wang, L.X. Zhao, Z. Li, C.S. Sun, T.M. Sun, Density functional theory (DFT) and natural bond orbital (NBO) study of vibrational spectra and intramolecular hydrogen bond interaction of L-ornithine–l-aspartate, Spectrochim. ActaA: Mol. Biomol. Spectrosc. 136 (2015) 338–346.

[33] G. Subhapriya, S. Kalyanaraman, N. Surumbarkuzhali, S. Vijayalakshmi, V. Krishnakumar, Investigation of intermolecular hydrogen bonding in 2,3,4,5,6 pentafluorobenzoic acid through molecular structure and vibrational analysis – A DFT approach, J. Mol. Struct 1083 (2015) 48–56.